ChemPubSoc Europe

DOI: 10.1002/chem.201704191

CHEMISTRY A European Journal Full Paper

Syngas Conversion

Cobalt-Iron-Manganese Catalysts for the Conversion of End-of-Life-Tire-Derived Syngas into Light Terminal Olefins

Jan P. Falkenhagen,[a] Lise Maisonneuve,[b] Pasi P. Paalanen,[a] Nathalie Coste,[b] Nicolas Malicki,[b] and Bert M. Weckhuysen*[a]

Abstract: Co-Fe-Mn/γ-Al_2O_3 Fischer–Tropsch synthesis (FTS) catalysts were synthesized, characterized and tested for CO hydrogenation, mimicking end-of-life-tire (ELT)-derived syngas. It was found that an increase of C_2-C_4 olefin selectivities to 49% could be reached for 5 wt% Co, 5 wt% Fe, 2.5 wt% Mn/γ-Al_2O_3 with Na at ambient pressure. Furthermore, by using a 5 wt% Co, 5 wt% Fe, 2.5 wt% Mn, 1.2 wt% Na, 0.03 wt% S/γ-Al_2O_3 catalyst the selectivity towards the fractions of C_{5+} and CH_4 could be reduced, whereas the selectivity towards the fraction of C_4 olefins could be improved to 12.6% at 10 bar. Moreover, the Na/S ratio influences the ratio of terminal to internal olefins observed as products, that is, a high Na loading prevents the isomerization of primary olefins, which is unwanted if 1,3-butadiene is the target product. Thus, by fine-tuning the addition of promoter elements the volume of waste streams that need to be recycled, treated or upgraded during ELT syngas processing could be reduced. The most promising catalyst (5 wt% Co, 5 wt% Fe, 2.5 wt% Mn, 1.2 wt% Na, 0.03 wt% S/γ-Al_2O_3) has been investigated using operando transmission X-ray microscopy (TXM) and X-ray diffraction (XRD). It was found that a cobalt-iron alloy was formed, whereas manganese remained in its oxidic phase.

Introduction

The Fischer–Tropsch synthesis (FTS) is a versatile production route for the conversion of syngas, that is, a mixture of CO and H_2, into high-quality fuels and waxes, which has been commercialized in various countries, including South Africa and Qatar.[1–14] Through pyrolysis or steam reforming, virtually all carbon sources, for example, natural gas, coal, waste, biomass as well as recycled rubber, can be converted into syngas to subsequently produce (renewable) fuels and chemicals.

Interestingly, currently large amounts of possible hydrocarbon feedstock, such as end-of-life tires (ELT), are poorly valorised and could be considered as a valuable source for syngas generation and subsequent FTS processing. In Europe, that is the EU27 as well as Norway, Switzerland and Turkey, the amount of ELT in 2012 was estimated to be equal to 3.6 million tons, of which 95% were recovered.[15] Of these 3.4 million tons of ELT, 37% were sent for energy recovery, whereas the vast majority was used by the cement industry to substitute mainly conventional fuel. However, 58% of the total ELT were re-used, either directly, retreaded or sent for material recovery. There, the tires are ground or shredded and the resulting granulates and powders are then commonly used for civil engineering applications, for example, in road construction or for erosion and sound barriers. This however has raised health concerns as toxic compounds (e.g., polycyclic aromatic hydrocarbons) have been detected in these final applications.[16] In other words, it would be advantageous if alternative application routes would be found for the use of these large amounts of ELT materials.

Interestingly, competing processes to valorize ELT, such as carbon substitution as used in the steel industry, de-vulcanization or pyrolysis, have yet to overcome a lot of challenges and do not see widespread application to date. In the case of pyrolysis, for example, the yielded products (i.e., solid char, pyrolytic liquids and gases) are often ill-defined and in turn their quality often does not justify the process costs. Hence, this process is used less and less because of oil prices-with a year-on-year reduction of 25% in 2012/2013.[15] Consequently, to circumvent these problems, it makes sense to look for alternative options to convert ELT into a high quality chemical feedstock. Here, syngas is a promising option because it opens up new synthesis routes towards fuels and important platform chemicals, such as methanol, ammonia or light olefins. The latter are especially interesting because the boom in the supply of non-

[a] Dr. J. P. Falkenhagen, P. P. Paalanen, Prof. Dr. B. M. Weckhuysen
Inorganic Chemistry and Catalysis
Debye Institute for Nanomaterials Science, Utrecht University
Universiteitsweg 99, 3584 CG Utrecht (The Netherlands)
E-mail: b.m.weckhuysen@uu.nl

[b] Dr. L. Maisonneuve, Dr. N. Coste, Dr. N. Malicki
Manufacture Française des Pneumatiques Michelin
Centre de Technologie de Ladoux
23 place des Carmes-Déchaux, 63040 Clermont-Ferrand (France)

Supporting information and the ORCID number(s) for the author(s) of this article can be found under https://doi.org/10.1002/chem.201704191.

© 2018 The Authors. Published by Wiley-VCH Verlag GmbH & Co. KGaA. This is an open access article under the terms of the Creative Commons Attribution-NonCommercial-NoDerivs License, which permits use and distribution in any medium, provided the original work is properly cited, the use is non-commercial and no modifications or adaptations are made.

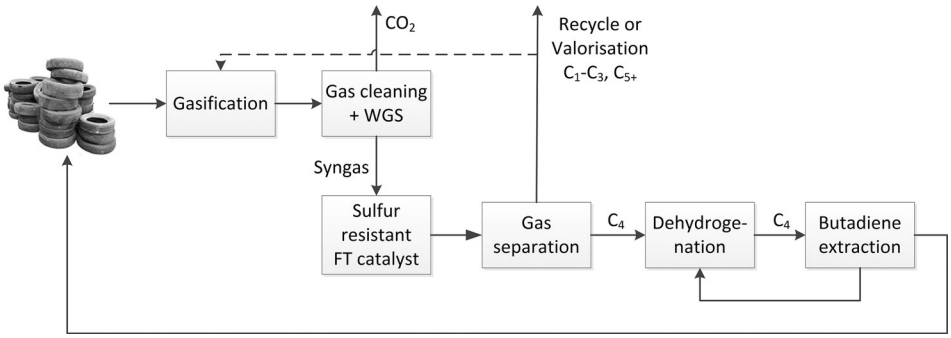

Figure 1. Block diagram for the conversion of synthesis gas derived from ELT into 1,3-butadiene for the production of synthetic rubbers for new tires, as explored in this research work. This includes the processing of potential recycle/valorisation streams, which should be minimized by increasing the selectivity towards light terminal olefins, including 1-butene, which can be further dehydrogenated to 1,3-butadiene. This approach requires the development of a sulfur-resistant Fischer–Tropsch-to-olefins (FTO) catalyst, which has a high selectivity towards C_4 olefins.

conventional oil sources in recent years has led to lighter hydrocarbon feedstocks and has reduced the global availability of important base chemicals, such as light olefins, including 1,3-butadiene. This creates opportunities for on-purpose processes because, for example, by 2025, 10% of the global butadiene production is expected to stem from the on-purpose dehydrogenation of 1-butene.[16]

The application of the FTS reaction to selectively produce light olefins from syngas has therefore gained a lot of interest recently and been named the Fischer–Tropsch-to-olefins (FTO) process.[17] With the help of FTO to produce 1-butene, followed by an additional catalytic dehydrogenation step, ELT-derived syngas could potentially thus be converted into 1,3-butadiene. This 1,3-butadiene can in principle then be re-used to produce new high-quality synthetic rubber for tires in a sustainable low-waste process, providing a closed carbon production circle. This approach, which we have explored in this research work, is illustrated in Figure 1. Fischer–Tropsch synthesis (FTS) is known to be catalyzed by Co- or Fe-based catalyst materials and extensive research has been carried out on these systems. Depending on the used catalyst and the related process conditions different reaction products are obtained.

In a high temperature (HT) regime (i.e., the HT-FTS process, $T = 320–350\,^{\circ}C$) Co-based catalysts would predominantly produce methane, whereas Fe-based catalysts mainly yield light olefins and paraffins. In a low temperature (LT) regime (i.e., the LT-FTS process, $T = 200–250\,^{\circ}C$), both for Co- and Fe-catalysts high molecular mass products are obtained, extending into the range of waxes. Moreover, Co is intrinsically more active than Fe[5,8] and consequently, finding a catalyst material that combines selectivities obtained in Fe-based processes with activities obtained in Co-based processes would represent a breakthrough.

However, making use of ELT-derived syngas poses serious challenges to a FTS process. Due to the vulcanization process, ELTs contain large amounts of S (typically 1.2–1.8 wt.%),[18] which has long been known as a poison for both Fe and Co FTS catalysts even when present in concentrations as low 1–2 $mg\,m^{-3}$.[19–24] Hence, the required clean-up of ELT-derived syngas to yield an appropriately low S content would become expensive. In contrast, early reports[25,26] claim that the addition of S (in combination with alkali elements) to catalysts based on Group 8 metals lengthened lifetime, increased olefin content and reduced the production of high boiling hydrocarbons, enhancing both activity and selectivity of the treated catalysts. This work has recently regained interest[24,27] and been extended to supported FTS catalysts.[28–31]

To date, most of the published studies focus on monometallic catalysts, which are catalysts featuring a single dominant FTS-active metal, with additional promotors to enhance activities and selectivities.[7] However, despite promising results only a limited number of studies on mixed bimetallic systems has been published.[32] Among these, bimetallic Fe-Co catalysts are of special interest because it has been shown that catalysts based on the combination of these elements may exhibit higher activities[33–37] or more favorable selectivities than their monometallic counterparts.[36,38]

In this work, we have synthesized a series of Co-Fe/γ-Al_2O_3 FTS catalysts with Na, Mn and S as additives for the production of lower terminal olefins, including 1-butene. We chose this combination of active elements and promotor elements to: (a) tune the product selectivity towards C_4 olefins at high temperature; (b) enhance the water–gas shift (WGS) reactivity, making it possible to use a H_2-poor syngas feed;[39] and (c) test the resistance of the catalysts towards poisoning through S-species, enabling the use of end-of-life tires derived syngas.

Hence, in this article, it will be shown that the fraction of C_4 olefins can be increased by adding Mn and Na as promoter elements. Moreover, we demonstrate that a high Na loading prevents the isomerization of primary olefins, which coincides with S enrichment in the catalyst material. Consequently, by adding Mn and Na as promoter elements, the expected yield towards C_4 olefins could be improved, and then the volume of by-products reduced. To get more fundamental insight into the nature of the active phase during FTS operation, operando transmission X-ray microscopy (TXM) and X-ray diffraction (XRD) has been used under realistic reaction conditions, that is, at 10 bar and 300 °C. It was found that a Co-Fe alloy was formed in the active catalyst, whereas Mn stayed in its oxidic state.

 © 2018 The Authors. Published by Wiley-VCH Verlag GmbH & Co. KGaA, Weinheim

Results and Discussion

Effect of the Co:Fe ratio and Mn promotion on catalyst selectivity and activity at atmospheric pressure

Table 1 shows the CO conversion, metal–time yields (MTY), and selectivities (CO_2-free) for a series of Co-Fe/γ-Al_2O_3 Fischer–Tropsch synthesis (FTS) catalysts under investigation in this work. These catalysts have been prepared with different Co:Fe:Mn ratios as well as in the presence and absence of Na and S as additives. Table S1 (Supporting Information) summarizes the elemental composition of the catalysts as well as their reduction behavior, as measured with temperature programmed reduction with hydrogen (H_2 TPR). The experiments were run under differential conditions at low conversion to exclude the interference of secondary reactions. The catalytic performances were collected after 8 h time on stream at atmospheric pressure, 270 °C and a H_2:CO ratio of 1:1. Here, in comparison to 2.5Co7.5Fe2.5Mn/γ-Al_2O_3 and 7.5Co2.5Fe2.5Mn/γ-Al_2O_3, 5Co5Fe2.5Mn/γ-Al_2O_3 shows a slightly higher metal–time yield (MTY) and C_4 olefin selectivity as well as lower methane selectivity. Interestingly, for these Mn-modified catalysts, a much less pronounced dependence of the selectivities on the Co:Fe ratio is observed than previously reported for Mn-free Co-Fe FTS catalysts.[38]

Effect of sodium and sulfur doping on catalyst selectivity and activity at atmospheric pressure

The effect of Na and S promotion on catalyst selectivity and activity was studied as well. Prior to the melt infiltration using the respective transition-metal nitrates, the γ-Al_2O_3 support was impregnated with a solution containing the appropriate amounts of ammonium sulfate and sodium nitrate. By following this procedure, it was ensured that the added S was adsorbed and distributed equally across the catalyst. Under the safe assumption that all S will be adsorbed,[24] the selected S loadings correspond to catalyst poisoning occurring in a typical Fe-based FTS plant under operating conditions employing syngas with a S content in the feed of typically <5 ppb over several years.[27] Comparing the results for the Na/S-doped FTS catalysts tested at atmospheric pressure, it is obvious that even adding small amounts of Na and S (i.e., 0.2 wt.%/0.06 wt.%, ca. 1 S atom per every 100 Co or Fe atoms in the catalyst) leads to significant changes in activity as well as the C_2, C_3 and C_4 olefin selectivity (Table 1). Furthermore, increasing the S content up to 0.12% (ca. 1 per 50 Co and Fe atoms) leads to a promotion effect rather than to catalyst poisoning. The activity (as expressed by the MTY) increases to 3.75×10^{-5} $mol_{CO}\cdot g_{metal}^{-1}\cdot s^{-1}$ for the best catalyst in this series (i.e., 5Co5Fe 2.5Mn0.2Na0.06S/γ-Al_2O_3), whereas a C_4 olefin selectivity of 14.8% is observed, compared to 4.6×10^{-5} $mol_{CO}\cdot g_{metal}^{-1}\cdot s^{-1}$ and a C_4 olefin selectivity of 13.9% for the sulfur-free catalysts (i.e., 5Co 5Fe2.5Mn/γ-Al_2O_3), respectively.

Similar behavior has been reported in the literature for Fe-based catalysts, whereas for Co-based systems, poisoning was observed.[24,27] However, because of the very different methods used (i.e., the use of spiked gas streams, impregnation of supported catalysts with S-containing solutions and co-precipitation or impregnation for bulk catalysts) the results remain difficult to compare. Nevertheless, Fe-based catalysts are relatively more resistant towards S poisoning, which can be explained through the more favorable formation of a cobalt sulfide phase in the case of Co-based catalysts.[24,40] For example, Co/Al_2O_3 poisoning has been reported for doping the material with as little as 10 ppm of sulfur (i.e., 1 S atom per 8300 Co atoms), when the catalyst was impregnated with an ammonium sulfide solution[41] or even lower levels when the feed gas was spiked with S-containing compounds.[42–45] Further increasing the Na loading in this series of catalysts to weight loadings beyond 0.2 wt.% leads to a shift in the chain length propagation factor, to an increase of the C_{5+} and to a decrease of the CH_4 selectivity together with a pronounced loss in activity.

Effect of Mn promotion on catalyst selectivity, activity and water–gas shift activity at 10 bar

To reach complete syngas conversion and to avoid gradients in the ratio of the partial pressures of the reactant gases over the reactor, the H_2/CO usage ratio of the catalytic reaction, calculated according to Equation (1),must match the H_2/CO feed ratio at the inlet of the reactor.

Table 1. Activity data for a series of Co-Fe-Mn/γ-Al_2O_3 FTS catalysts after 8 h time on stream at atmospheric pressure, 270 °C and a H_2:CO ratio of 1:1.

Catalyst	Conversion [%]	MTY [10^{-5} mol CO·g_m^{-1}·s^{-1}]	Selectivity [%]					
			CH_4	C_2-C_3O	C_2-C_3P	C_4O	C_4P	C_{5+}
2.5Co7.5Fe2.5Mn	0.8	0.9	24.7	34.7	0.9	12.8	0.7	26.2
5Co5Fe2.5Mn	2.1	2.3	23.7	32.6	0.7	13.9	0.5	28.6
7.5Co2.5Fe2.5Mn	2.1	2.3	24.4	31.6	0.9	13.5	0.6	29.0
5Co5Fe2.5Mn								
0.2Na0.06S	3.4	3.7	23.1	34.4	2.0	14.8	0.7	24.9
0.2Na0.12S	3.0	3.3	23.4	33.8	3.4	15.4	1.0	23.0
0.4Na0.09S	2.1	2.3	19.8	34.8	1.5	14.9	0.6	28.2
0.6Na0.03S	0.6	0.7	14.0	28.8	0.7	15.6	0.6	40.2
0.6Na0.09S	1.5	1.7	19.1	33.4	1.0	15.0	0.5	30.6
1.2Na0.03S	0.8	0.9	18.6	29.5	0.7	14.6	0.6	35.8

 © 2018 The Authors. Published by Wiley-VCH Verlag GmbH & Co. KGaA, Weinheim

$$\text{Usage ratio} = \frac{\text{mol}H_2\text{in} - \text{mol}H_2\text{out}}{\text{mol}CO\text{in} - \text{mol}CO\text{out}} \quad (1)$$

For catalysts having no water–gas shift activity, according to Equation (2), the observed usage ratio is around 2.1, as determined by the stoichiometry of the FTS reaction itself.[4] Making use of a catalyst, that is active for the WGS reaction, allows the use of lower H_2/CO ratios in the syngas feed, for example, H_2-poor syngas as usual syngas derived from biomass or as one may expect from rubber gasification.[39]

$$CO + H_2O \leftrightarrow CO_2 + H_2 \quad (2)$$

Here, a supported Co-Fe catalyst could be expected to combine beneficial properties of both Co and Fe catalysts exhibiting both a high FTS and WGS activity. However, previous studies have shown, that under the conditions used for the LT-FTS process (up to 250 °C) WGS activities of Co:Fe catalyst materials are negligible.[4,36,38,46] Thus, to improve the WGS activity, manganese oxide has been added to the catalyst materials as a potential chemical promoter[10] and the catalytic studies were conducted at a higher temperature.

Table 2 summarizes the catalytic data of a series of Co-Fe-Mn/γ-Al_2O_3 FTS catalysts. The conversion, the hydrocarbon yield, the usage ratio and the time yields for the different Co-Fe-Mn/γ-Al_2O_3 catalysts have been investigated under industrially relevant conditions at 10 bar and 300 °C. Under these conditions, the catalyst materials under investigation reach intermediate conversion levels between 39 and 65% and selectivities towards CO_2 of 30–37%, proving that the Co-Fe-Mn/γ-Al_2O_3 catalysts are indeed active for promoting the WGS reaction. Moreover, the observed usage ratios are in the range of 1.3–1.4 and therefore well below the expected stoichiometric ratio and the ratio used in a typical industrial process.[36] The first trend that becomes obvious from Table 2 is that for the Mn-promoted Fe-Co catalysts at 10 bar, the conversion and the MYTs increase with increasing cobalt content. This trend is more pronounced at 10 bar than at atmospheric pressure. Compared to the results for the tests run at atmospheric pressure, the selectivities towards lower olefins observed at 10 bar are significantly reduced for all catalysts tested. Furthermore, the olefinicity of the lighter hydrocarbon fractions is reduced, hinting towards a higher influence of secondary hydrogenation reactions at higher pressure. In agreement with a higher chain length propagation probability, a higher amount of C_{5+} fractions is observed. It is evident that compared to the 2.5Co7.5Fe2.5Mn/γ-Al_2O_3 and 7.5Co2.5Fe2.5Mn/γ-Al_2O_3 catalyst materials, 5Co5Fe2.5Mn/γ-Al_2O_3 exhibits reduced selectivities towards the (Figure 1) undesired CH_4, C_2-C_3 and C_4P fractions (Table 3) and increased C_{5+} selectivity. Moreover, the selectivity towards the desired C_4 olefin fraction, including 1-butene, is similar for the three catalysts. Looking more closely at the product distribution towards individual C_4 components within the C_4 olefin fraction, the 5Co5Fe2.5Mn/γ-Al_2O_3 catalyst is more selective towards 1-butene as the desired terminal olefin and less selective towards internal olefins (i.e., *cis*- and *trans*-2-butene). Based on the hydrocarbon yields per time unit for the tested catalyst materials (Table 4), 5Co5Fe2.5Mn/γ-Al_2O_3 was selected as the most promising candidate for further optimization due to its comparably high 1-butene productivity as well as its low productivity towards internal olefins and branched C_4 hydrocarbons and its intermediate CH_4 productivity.

Table 2. Activity data for promoted, unpromoted and partially poisoned Co-Fe-Mn/γ-Al_2O_3 catalysts after 24 h on stream at 10 bar, 300 °C, a H_2/CO ratio of 1:1 and a GHSV of 4000 $mL_n \cdot g_{cat}^{-1} \cdot h^{-1}$.

Catalyst	Conversion [%]	HC yield [$gHC \cdot kg_{cat}^{-1} \cdot h^{-1}$]	Usage ratio [mol_{H_2}/mol_{CO}]	MTY [10^{-4} $mol \cdot g_{metal}^{-1} \cdot s^{-1}$]	CO_2 [%]
2.5Co7.5Fe2.5Mn	39.4	248	1.3	0.8	37.1
5Co5Fe2.5Mn	54.5	381	1.4	1.1	30.1
7.5Co2.5Fe2.5Mn 5Co5Fe2.5Mn	64.8	438	1.3	1.3	32.0
0.2Na0.06S	41.7	285	1.5	0.8	31.2
0.2Na0.12S	32.9	223	1.6	0.6	31.4
0.4Na0.09S	35.3	235	1.5	0.7	33.3
0.6Na0.03S	44.0	289	1.4	0.9	33.8
0.6Na0.09S	29.7	172	1.5	0.6	41.8
1.2Na0.03S	44.1	247	1.0	0.9	43.6

Table 3. Selectivities for promoted, unpromoted and partially poisoned Co-Fe-Mn/γ-Al_2O_3 catalysts after 24 h on stream at 10 bar, 300 °C, a H_2/CO ratio of 1:1 and a GHSV of 4 $L_n \cdot g_{cat}^{-1} \cdot h^{-1}$.

Catalyst	Selectivity [%C]													
	CH_4	C_2O	C_2P	C_3O	C_3P	C_4O	C_4P	C_{5+}	iso-Butane	*n*-Butane	*trans*-2-Butene	1-Butene	iso-Butene	*cis*-2-Butene
2.5Co7.5Fe2.5Mn	25.8	0.8	6.7	9.3	3.3	8.2	2.8	43.0	0.1	2.7	1.6	4.3	0.6	1.6
5Co5Fe2.5Mn	19.4	0.8	3.6	7.9	1.7	8.0	1.8	56.9	0.0	1.7	1.1	5.2	0.5	1.2
7.5Co2.5Fe2.5Mn 5Co5Fe2.5Mn	23.9	0.7	4.1	9.3	2.0	9.2	2.1	48.7	0.0	2.1	1.5	5.5	0.5	1.6
0.2Na0.06S	25.1	0.8	8.2	10.8	7.0	11.9	4.7	31.5	0.1	4.6	4.2	3.4	0.9	3.4
0.2Na0.12S	26.5	0.9	9.0	10.0	8.8	11.6	5.3	27.8	0.3	5.1	4.6	2.7	1.0	3.3
0.4Na0.09S	23.9	0.9	8.3	11.4	6.7	12.1	4.3	32.3	0.1	4.1	4.4	3.4	1.0	3.3
0.6Na0.03S	21.4	1.2	6.0	11.8	3.3	11.8	3.0	41.6	0.0	3.0	2.5	6.0	0.8	2.5
0.6Na0.09S	26.2	1.3	10.2	14.0	7.7	14.5	4.9	21.3	0.0	4.9	4.9	4.2	1.3	4.1
1.2Na0.03S	18.1	2.0	6.6	13.5	3.0	12.6	2.8	41.4	0.1	2.7	2.1	7.2	0.9	2.3

 © 2018 The Authors. Published by Wiley-VCH Verlag GmbH & Co. KGaA, Weinheim

Table 4. Hydrocarbon yields for promoted, unpromoted and partially poisoned 5Co5Fe2.5Mn/γ-Al_2O_3 catalyst materials catalysts after 24 h on stream at 10 bar, 300 °C, a H_2/CO ratio of 1:1 and a GHSV of 4000 $mL_n \cdot g_{cat}^{-1} \cdot h^{-1}$.

	Hydrocarbon yield [$g_{HC} \cdot kg_{cat}^{-1} \cdot h^{-1}$]															
	CH_4	C_2O	C_2P	C_3O	C_3P	C_4O	C_4P	C_{5+}	iso-Butane	*n*-Butane	*trans*-2-Butene	1-Butene	iso-Butene	*cis*-2-Butene	C_2-C_4O/[HC-(C_2-C_4O)]	1-butene/C_2-C_4O
2.5Co7.5Fe2.5Mn	73.3	2.0	17.9	23.0	8.6	20.3	7.3	95.2	0.2	7.1	4.0	10.7	1.5	4.0	0.22	0.24
5Co5Fe2.5Mn	84.6	3.1	14.6	30.1	6.6	30.7	6.9	204.7	0.2	6.8	4.3	19.9	1.7	4.6	0.20	0.31
7.5Co2.5Fe2.5Mn 5Co5Fe2.5Mn	119.7	3.2	19.4	40.7	9.4	40.3	9.5	195.5	0.2	9.4	6.7	24.2	2.3	7.0	0.24	0.29
0.2Na0.06S	82.1	2.2	25.2	31.0	21.0	33.9	13.9	76.0	0.3	13.6	12.0	9.7	2.6	9.6	0.31	0.14
0.2Na0.12S	67.8	2.0	21.6	22.4	20.6	26.0	12.4	50.5	0.6	11.8	10.3	6.1	2.2	7.4	0.29	0.12
0.4Na0.09S	64.4	2.2	21.0	26.8	16.5	28.5	10.4	65.0	0.3	10.1	10.3	8.1	2.3	7.9	0.32	0.14
0.6Na0.03S	70.8	3.6	18.6	34.1	10.0	34.1	8.9	109.1	0.0	8.9	7.1	17.2	2.2	7.2	0.33	0.24
0.6Na0.09S	51.6	2.2	18.8	24.1	13.9	25.0	8.7	27.7	0.0	8.7	8.5	7.3	2.2	7.0	0.47	0.14
1.2Na0.03S	51.1	4.9	17.5	33.5	7.9	31.1	7.1	93.9	0.2	6.9	5.2	17.8	2.3	5.6	0.39	0.26

Effect of sodium and sulfur doping on catalyst selectivity and activity at 10 bar

In a next step of our study, a set of 5Co5Fe2.5Mn/γ-Al_2O_3 catalyst materials based on a γ-Al_2O_3 support doped with different absolute levels and ratios of Na and S was investigated. Depending on the respective catalyst, conversion levels between 30 and 44% were achieved-compared to 55% for the Na/S-free 5Co5Fe2.5Mn/γ-Al_2O_3 catalyst (Table 2). Here, the poisoning effect on the catalyst activity due to S doping is partly compensated by a positive influence due to an increasing Na loading. For the usage ratios, with the notable exception of 5Co5Fe2.5Mn1.2Na0.03S/γ-Al_2O_3, values between 1.4 and 1.6 are observed. Interestingly, lower usage ratios are achieved with catalyst materials, which are rich in Na, whereas an opposing trend is observed with regard to S doping.

Table 3 summarizes the selectivities for the different studied catalysts. It was found that the CH_4 selectivity, exhibited by the Na/S doped catalysts, while initially being higher than for the Na/S-free catalysts drops with increasing Na content. With an increasing Na/S promoter ratio, both the olefinicity of this fraction (Figure 2) and the absolute selectivity towards C_2-C_3 hydrocarbons increase significantly, especially compared to the Na/S-free samples. Most importantly, for the Na/S-doped catalyst materials, the selectivity towards the desired C_4 olefin fraction is improved from 8.0% in the Na/S-free 5Co5Fe2.5Mn/γ-Al_2O_3 material to 12.6% in the 5Co5Fe2.5Mn1.2Na0.03S/γ-Al_2O_3 sample, whereas the C_{5+} selectivity is reduced. This corresponds to a marked reduction in the hydrocarbon yields (Table 4) for the CH_4 and the C_{5+} fractions, whereas the C_4 olefin productivity is maintained at 0.03 $kg \cdot kg_{cat}^{-1} \cdot h^{-1}$.

For the distribution of individual compounds within the C_4 fraction, there is a clear trend that the amount of formed terminal olefins increases with an increasing Na/S ratio, whereas a lower ratio leads to higher amounts of internal olefins (Figure 2). Chemically, this can be rationalized as a reduction of acidity of the alumina support due to the promotion with Na and therefore a reduced activity of the support material for olefin isomerization.[47,48] Therefore, adding Na to the catalyst materials helps to preserve the catalytic performance from poisoning by S, inhibiting the isomerization of terminal olefins on the catalyst support.

Active phase determination with operando transmission X-ray microscopy (TXM) and X-ray diffraction

As TXM beamtime is very precious, we have made a selection process to determine which catalyst should be investigated with this method. Two different metrics were used keeping the

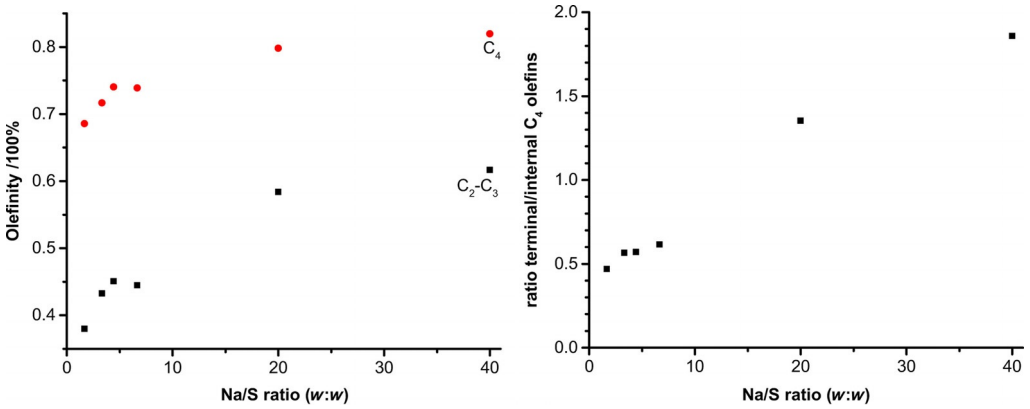

Figure 2. Relationship between the Na/S ratio and the ratio of terminal and internal olefins (left); the olefinicity of C_2-C_3 and C_4 product fractions, respectively for a series of 5Co5Fe2.5Mn/γ-Al_2O_3 catalyst materials (right).

© 2018 The Authors. Published by Wiley-VCH Verlag GmbH & Co. KGaA, Weinheim

overall aim as expressed in Figure 1 in mind. To reduce the volume of waste streams of little value in an industrial process, the CH_4, C_2–C_4 paraffin and C_{5+} hydrocarbon fractions should be suppressed, whereas a maximum yield of C_2–C_4 olefins (C_2-C_4O) is desired. That is, the yield ratio of valuable C_2–C_4O streams compared to waste streams [all hydrocarbons produced with the exception of C_2–C_4 olefins: C_2-C_4O/(HC-(C_2-C_4O)] should be improved. Here, the two best performing catalyst materials are 5Co5Fe2.5Mn0.6Na0.09S/γ-Al_2O_3 and 5Co5-Fe2.5Mn1.2Na 0.03S/γ-Al_2O_3, respectively (Table 4). At the same time, 1-butene is especially suitable for further conversion to 1,3-butadiene by catalytic dehydrogenation (e.g., by the Mitsubishi butene to crude butadiene (BtcB) process), which makes it the most valuable component of the C_4 stream in our approach offering an alternative to established processes for the production of 1,3-butadiene.[49–53] Therefore, a maximum 1-butene yield within the C_4 olefin fraction is desired and as a secondary metric the ratio of 1-butene/C_2-C_4O can be used to identify the most promising catalyst. From Table 4, it is evident that in this domain, 5Co5Fe2.5Mn1.2Na0.03S/γ-Al_2O_3 is performing significantly better than 5Co5Fe2.5Mn0.6Na0.09S/γ-Al_2O_3, making it the best choice for further characterization. Therefore, 5Co5Fe2.5Mn 1.2Na0.03S/γ-Al_2O_3 was selected for the operando TXM study.

To compromise between measurement time and data quality, energy points were selected so that the recording time of each scan was approximately 30 min. Before the operando TXM experiment started the fresh catalyst was characterized at room temperature by measuring Mn, Fe and Co K-edge TXM image stacks. For the identification and quantification of Co, Fe and Mn species, present bulk X-ray absorption near-edge structure (XANES) spectra (Figures S1–S4 in the Supporting Information) were generated by averaging all pixels. The data was least squares fitted to the spectra of Co, Fe and Mn reference materials. A full list of Co, Fe and Mn species, which were considered to be present during the experiment together with their XANES spectra, is included in the Supporting Information (Figures S5–S7).

For the fresh catalyst sample the quantification of the present Mn phases yields a mixture of predominantly Mn^{III} and Mn^{IV} and oxide phases with a Mn/O ratio of 1.7 (Figure 3), which is in line with characterization results earlier published for manganese nitrate-derived Mn/γ-Al_2O_3 catalyst materials.[54] Under reducing conditions, this composition changes during temperature ramping to 400 °C within 30 min to give about a 65/35 mixture of manganosite and Mn_3O_4, therefore a mixture of Mn^{II} and Mn^{III} species.[55] This ratio remains almost constant during reduction and FTS, confirming the presence of oxidic Mn species, which are known to catalyze the WGS reaction.[56,57]

In the fresh catalyst material, Fe is exclusively present in the oxidation state 3+, both as maghemite and hematite in a ratio of around 80/20. However, due to the large similarities of the XANES spectra of hematite and $Co_xFe_xO_4$ spinels, a clear distinction between these materials is not possible from our data.[58] Co species are found as a mixture of both Co^{II} and Co^{III} species, namely in $CoFe_2O_4$ and Co_3O_4 phases. This is corroborated by XRD measurements, in which differences in the XRD patterns for the Co_3O_4 and $CoFe_2O_4$ phases are observed (Figures S8–S10, Supporting Information).

As soon as the catalyst is heated in a stream of H_2 and He, reduced phases are observed. After the reduction at a constant temperature of 400 °C, the majority of both Co (59%) and Fe atoms (70%) are then reduced to their metallic state, probably forming an alloy, which could be confirmed by operando XRD measurements (Figure S**11**), making use of a laboratory set-up developed recently in our laboratory.[63] In both cases, little change is seen between the two datasets recorded at different times during the reduction indicating that the process was complete after the first spectrum was recorded. However, partially reduced metal(II) oxide species (i.e., FeO and CoO), which could stem from very small particles exhibiting strong metal support interactions (SMSI) were still detected. In the case of Fe, even a FeS_x species is observed, which could stem from the S that was added to the catalyst during impregnation or impurities in the syngas feed. After the reduction phase the temperature of the reactor was lowered and the system was pressurized with syngas (H_2:CO 1:1) to 10 bar. At this point the mass spectrometric analysis of the effluent gas from the reactor demonstrates that methane, ethylene, ethane and propane were formed in the FTS reaction (Figure S12, Supporting Information), that is, a working catalyst was truly studied in this operando TXM experiment.

The least square fits for both the Fe and the Co K-edge spectra indicate that the present phases in the catalyst shift upon introduction of syngas into the reactor. For Fe, the major species is still Fe metal with a contribution of about 59–64%, whereas wüstite and maghemite contribute about 25–28% and around 12–13%, respectively. For Co, most of the contribution to the fitted data stems from Co metal (≈70–77%), whereas the remaining amount consists of CoO (≈23–30%). Thus, the spectral fits both for the Fe and Co K-edge XANES spectra demonstrate that the degrees of reduction of the Fe and Co phase remain similar upon exposure to syngas.

From 2D TXM, further conclusions can be drawn (Figure 3). In the fresh catalyst material, Co, Fe and Mn are seemingly homogeneously distributed across the section of the measured catalyst particle that is in the field of view (FOV) (ca. 25× 25 μm) of the performed TXM experiment. The fact that Mn seems to be concentrated in the center part of the catalyst particle is due to the spherical shape of the particle, that is, the sample thickness increases from the top-left to the bottom-right corner of the FOV. Because of the low 2.5 wt.% loading of Mn on the material pixels in the shell region are filtered out. Thus, to extract the most relevant chemical information, regions of interest (indicated as white squares) were used for pixel averaging to yield the XANES spectra. The fresh catalyst particle consists of Co_3O_4 and $CoFe_2O_4$, Fe_2O_3 (both as hematite and maghemite), MnO_2, Mn_3O_4 and Mn_2O_3 (Figure 3). In the initial phase during the temperature ramp, the reduction of the Co species does not occur completely homogeneously (Figure S2, Supporting Information). However, no clear difference between catalyst particle core and shell was observed. With proceeding reduction, the local differences become much

 © 2018 The Authors. Published by Wiley-VCH Verlag GmbH & Co. KGaA, Weinheim

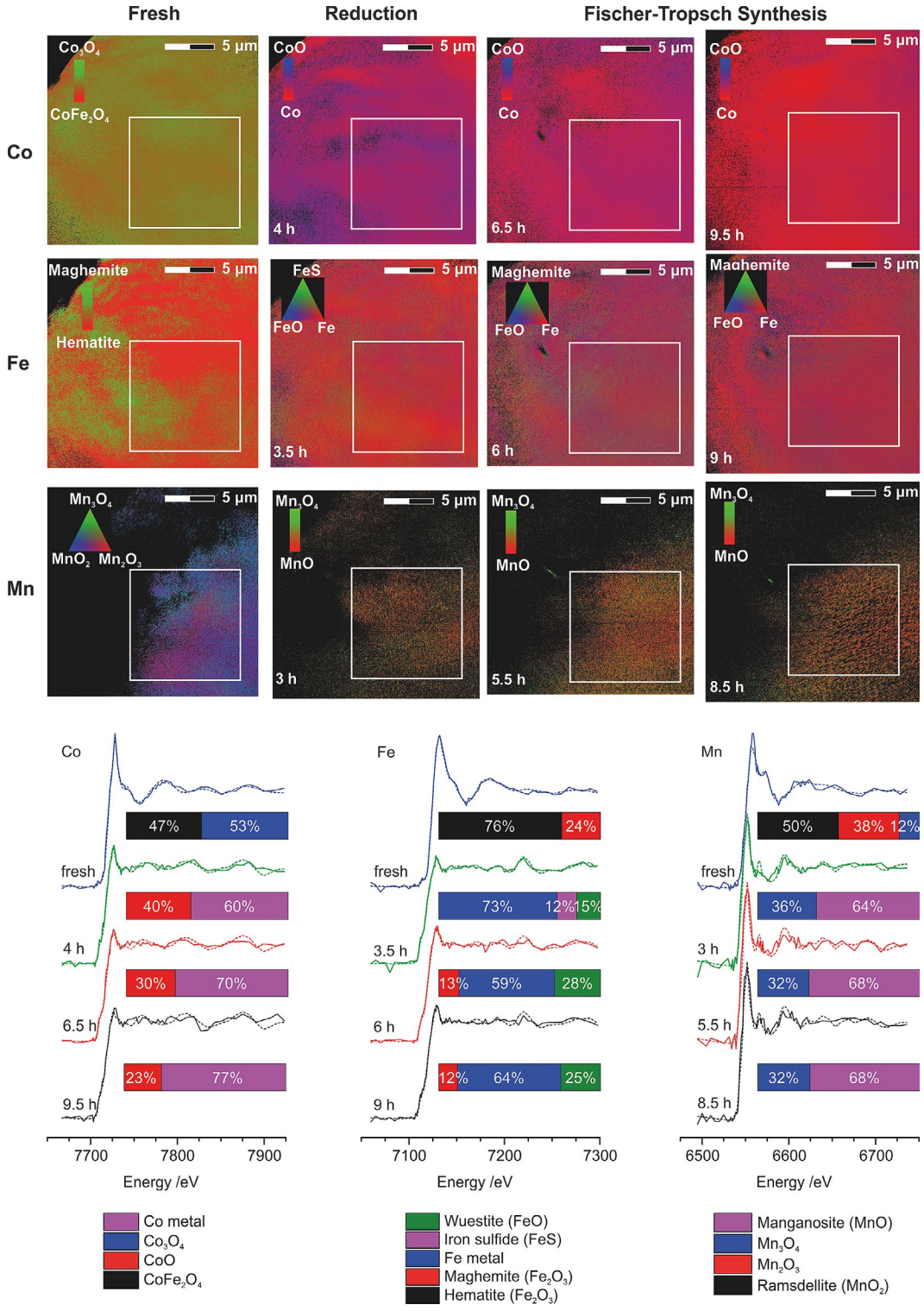

Figure 3. Top: A series of 2D TXM images of a 5Co5Fe2.5Mn1.2Na0.03S/γ-Al_2O_3 catalyst particle as a function of the different treatments applied: fresh material at room temperature; during reduction; during FTS at 300 °C and 10 bar pressure in syngas with a H_2/CO of 1:1. The white squares highlight the regions of interested, which were used for generating the XANES spectra. The times-on-stream are stated as inside the respective images. Bottom: Co, Fe and Mn bulk XANES spectra (solid lines) together with their least-squares fits (dashed lines) during the in situ experiment. Co, Mn and Fe-K edge phase quantification was obtained by fitting the obtained bulk XANES spectra with spectra of reference compounds.

less pronounced and the investigated metal species become almost homogeneously distributed across the particle.

Conclusion

A series of Co-Fe-Mn/γ-Al_2O_3 materials was synthesized and tested as catalysts for Fischer–Tropsch synthesis (FTS). The aim

© 2018 The Authors. Published by Wiley-VCH Verlag GmbH & Co. KGaA, Weinheim

was to use S-rich end-of-life-tire (ELT)-derived syngas with a low H_2/CO ratio of 1:1 to facilitate the production of lower olefins, including 1-butene.[39] It was assumed that MnO_x should act here as water–gas shift (WGS) catalyst, as was proposed in our past work on Co-Mn/TiO_2 FTS catalysts.[55,56,64,65] However, for these Co-Mn/TiO_2 FTS catalysts, it was already found that the role is complex as MnO_x was considered to be both a structural and electronic promotor, resulting in higher metal dispersions and lower hydrogenation activity. These findings are in line with a recent paper of Han and co-workers who found that the addition of MnO_x to a Fe/SiO_2 FTS catalyst increased the reaction rate (by for example, enhancing the dissociation adsorption of CO) and the olefin selectivity.[66] Furthermore, these authors observed that MnO_x improved the dispersion of supported FeO_x, facilitating its reduction and enhancing the carburization of FeO_x. Interestingly, Xiaohao and co-workers have recently investigated the addition of MnO_x to a Co/SiO_2 FTS catalyst.[67] These authors found that MnO_x affects the formation of Co_2C, a phase which has been recently shown to have a high selectivity towards lower olefins.[68]

In our current work, it was further found that by doping a 5Co5Fe2.5Mn/γ-Al_2O_3 material with additional 1.2 wt.% of Na and 0.03 wt.% of S, the selectivity towards C_4 olefins could be significantly improved, whereas, compared to the Na/S-free catalysts, C_{5+} and CH_4 fractions are reduced at a comparable C_4 olefin productivity of 0.03 $kg \cdot kg_{cat}^{-1} \cdot h^{-1}$. Furthermore, the Na/S ratio has been identified as a factor influencing the isomerization of 1-alkenes. Thus, by adding Na as a promoter, the isomerization of 1-alkenes can be inhibited and the ratio of 1-alkenes to internal and iso-alkenes is maintained even if S is present. In other words, under S-rich conditions, the selectivity can be directed towards the target product 1-butene as the primary product in the C_4 olefin fraction and therefore the amount of waste streams that need to be recycled, treated or upgraded is reduced.

TXM has been used to chemically image a single 5 wt% Co, 5 wt% Fe, 2.5 wt% Mn, 1.2 wt% Na, 0.03 wt% S/γ-Al_2O_3 catalyst particle with a spatial resolution of about 30 nm in 2D and to identify, localize and quantify the Co, Fe and Mn species present. These TXM measurements have been carried out for the fresh catalyst material and both during catalyst activation and under FT synthesis conditions. The initial reduction leads to a fast formation of a homogeneously distributed cobalt-iron alloy as the active catalytic phase, which could be confirmed by a separate operando XRD experiment. Furthermore, it was found that manganese stays oxidic during FTS.

Experimental Section

Catalyst synthesis: Supported catalysts with a nominal metal loading of 10 wt% (Fe and Co combined) were prepared by incipient wetness impregnation and melt infiltration. First, aqueous solutions of appropriate concentrations of $NaNO_3$ and NH_4SO_4 were used to fill the pores of aliquots (1.00 g) of the γ-Al_2O_3 (170 $m^2 g^{-1}$, pore volume 0.44 $mL g^{-1}$, Puralox SCCa 5/170, Sasol Germany) support material. The materials were then dried at 100 °C (2 h) in flowing air and calcined at 400 °C (2 °C min^{-1}, 8 h). In a second step, these materials were infiltrated with a melt of appropriate amounts of the transition-metal nitrate precursors at 63 °C. The materials were then dried and calcined. The catalyst samples have been characterized by temperature programmed reduction (TPR) with H_2 and the experimental details as well as the data are summarized in Table S1 and Figure S13 (Supporting Information).

Catalyst testing: Atmospheric pressure catalytic experiments were carried out in a fixed bed reactor and kept to conversions $< 5\%$ to ensure differential operation of the catalyst bed. A H_2/CO feed ratio of 1 and a GHSV (Gas Hourly Space Velocity) of 18 $L_n \cdot g_{cat}^{-1} \cdot h^{-1}$ were used. 20.0 mg of the calcined catalysts (75–150 μm sieve fractions) were diluted with 80.0 mg of silicon carbide (75–150 μm sieve fractions) and pre-reduced in pure H_2 at 400 °C (1 °C min^{-1}, 16 h, 60 $L_n \cdot g_{cat}^{-1} \cdot h^{-1}$). The temperature was lowered and syngas was introduced into the reactor. Results after 8 h on stream at 270 °C are reported. The produced hydrocarbons were quantified using a Varian CP-3800 GC equipped with a FID detector. For calculating the performance hydrocarbon fractions from C_1 to C_{10} were analysed. Selectivities are calculated free from CO_2; % C represents the percentage of carbon atoms in a product fraction with respect to all converted CO molecules. Metal–time yield (MTY) is defined as mol of CO converted to hydrocarbons per gram of cobalt/iron.

10 bar catalytic experiments were conducted employing a custom-built fixed bed reactor. Here, a quartz reactor tube with an inner diameter of 6 mm was used. Typically 150 mg of catalyst were diluted with SiC to give a bed length of 30 mm. Catalysts were pre-reduced (1 °C min^{-1}, 400 °C, 12 h) at ambient pressure using a 90/10 H_2/He mixture with a GHSV of 22 $L_n \cdot g_{cat}^{-1} \cdot h^{-1}$, the reactor was then cooled to 210 °C at which point it was pressurized with syngas (H_2/CO/He 40:40:20) to reach 10 bar. The GHSV was then reduced to 4 $L_n \cdot g_{cat}^{-1} \cdot h^{-1}$ and the temperature raised to 300 °C (2 °C min^{-1}). For the analysis of products a modified Thermo Scientific Trace 1300 GC with one FID (C_1–C_5, C_{6+}) and two TCD channels (for permanent gases) was used. He was used as an internal standard to calculate the flow through the reactor. This flow was then used to determine the conversion, productivities and selectivities. The selectivities towards the hydrocarbon products are given free from CO_2. Some details on these catalytic experiments, including a chromatographic analysis of the product composition, are shown in Figures S14 and S15 in the Supporting Information.

Catalyst characterization: TXM has been conducted on the Beamline 6-2c at the Stanford Synchrotron Radiation Lightsource (SSRL) at SLAC/Stanford University (Menlo Park, CA, USA).[59] In TXM, monochromatic X-radiation from the synchrotron source is focused onto the sample by a capillary condenser. The transmission image is formed by a zone plate onto a CCD camera. The image has an energy dependent field of view of about 25 μmx25 μm and a spatial resolution of about 30 nm. By changing the energy during imaging, XANES spectra are collected for each pixel. These XANES spectra give information about the local chemical environment and oxidation states of the element(s) of interest, that is., Fe, Mn and Co. For this experiment, FTS catalyst particles are placed in a thin-walled borosilicate glass capillary with a diameter of 200 μm and a wall thickness of 10 μm, which is attached to a custom made reactor holder. The particles are held in place within the isothermal zone of the reactor by glass wool fibres, which also keep them separate to allow overlap-free imaging of the particles. The holder is then placed inside an oven with two windows, which are covered with aluminium foil allow the X-ray radiation to reach the reactor and the detector. A description of the operando TXM system has been reported in previous articles from our group.[60–63] The catalyst was pre-reduced in a stream of H_2 and He 90/10 (*v*:*v*) at 400 °C and 0.5 bar (10 °C min^{-1}, 4 h), then the reactor was cooled

 © 2018 The Authors. Published by Wiley-VCH Verlag GmbH & Co. KGaA, Weinheim

to 210 °C; syngas (H_2/CO/He, 45/45/10) was introduced and the system was pressurized to 10 bar, whereas the reactor was heated to 300 °C (5 °C min^{-1}, 4.5 h). Before the reaction, as well as during reduction and the FTS reaction, XANES spectra at the Mn, Fe and Co, K-edges were measured; during temperature ramping XANES spectra at the Co K-edge were also recorded. During the FTS experiment, mass spectra were recorded using a Pfeiffer Vacuum OmniStar GSD 320 quadrupole mass spectrometer using the built-in Faraday detector, making it a truly operando experiment.

Acknowledgements

This project has been funded by the Michelin Group. The authors thank Oscar Kerkenaar (Utrecht University, UU) for the help in constructing the Fischer–Tropsch synthesis setup. The help of Ramon Oord (UU) and Matthias Filez (UU) during the TXM beamtime is highly appreciated. Part of this research was carried out at the Stanford Synchrotron Radiation Lightsource (SSRL), a Directorate of SLAC National Accelerator Laboratory and an Office of Science User Facility operated for the U.S. Department of Energy Office of Science by Stanford University.

Conflict of interest

The authors declare no conflict of interest.

Keywords: cobalt · Fischer–Tropsch synthesis · iron · manganese · transmission X-ray microscopy

[1] M. Argyle, C. Bartholomew, *Catalysts* **2015**, *5*, 145 – 269.
[2] a) C. H. Bartholomew, *Catal. Lett.* **1991**, *7*, 303 – 316; b) M. A. Vannice, *J. Catal.* **1975**, *37*, 449 – 461; c) M. A. Vannice, *J. Catal.* **1975**, *37*, 462 – 473; d) D. Fu, W. Dai, Xi. Wu, W. Mao, J. Su, Z. Zhang, B. Shi, J. Smith, P. Li, J. Xu, Y. F. Han, *ChemCatChem* **2015**, *7*, 752 – 756.
[3] F. Diehl, A. Y. Khodakov, *Oil Gas Sci. Technol.* **2009**, *64*, 11 – 24.
[4] M. E. Dry, *Catal. Today* **2002**, *71*, 227 – 241.
[5] M. E. Dry, *Appl. Catal. A* **1996**, *138*, 319 – 344.
[6] G. W. Huber, S. Iborra, A. Corma, *Chem. Rev.* **2006**, *106*, 4044 – 4098.
[7] F. Morales, B. M. Weckhuysen, in *Catalysis* (Ed.: J. J. Spivey), Royal Society Of Chemistry, Cambridge, **2006**, pp. 1 – 40.
[8] J. van de Loosdrecht, F. G. Botes, I. M. Ciobica, A. Ferreira, P. Gibson, D. J. Moodley, A. M. Saib, J. L. Visagie, C. J. Weststrate, J. W. Niemantsverdriet, in *Compr. Inorg. Chem. II*, Elsevier, Amsterdam, **2013**, pp. 525 – 557.
[9] E. van Steen, M. Claeys, *Chem. Eng. Technol.* **2008**, *31*, 655 – 666.
[10] E. de Smit, B. M. Weckhuysen, *Chem. Soc. Rev.* **2008**, *37*, 2758 – 2781.
[11] E. Iglesia, *Appl. Catal. A* **1997**, *161*, 59 – 78.
[12] A. Y. Khodakov, W. Chu, P. Fongarland, *Chem. Rev.* **2007**, *107*, 1692 – 1744.
[13] G. Van Der Laan, A. Beenackers, *Catal. Rev.* **1999**, *41*, 255 – 318.
[14] Q. Zhang, J. Kang, Y. Wang, *ChemCatChem* **2010**, *2*, 1030 – 1058.
[15] Etrma, ETRMA Annual Report 2013/2014, **2014**.
[16] A. Ibbotson, C. Lopes, in *34th Lat. Am. Petrochemical Annu. Meet.* **2014**.
[17] H. M. Torres Galvis, K. P. de Jong, *ACS Catal.* **2013**, *3*, 2130 – 2149.
[18] S. Lee, in *Handb. Altern. Fuel Technol.* (Eds.: S. Lee, J. G. Speight, S. K. Loyalka), CRC Press, Boca Raton, **2015**, pp. 542.
[19] M. E. Dry, in *Catal.- Sci. Technol.* (Eds.: J. R. Anderson, M. Boudart), Springer, Berlin, **1981**, pp. 159 – 255.
[20] R. B. Anderson, F. S. Karn, J. F. Shultz, *J. Catal.* **1965**, *4*, 56 – 63.
[21] F. S. Karn, J. F. Shultz, R. E. Kelly, R. B. Anderson, *Ind. Eng. Chem. Prod. Res. Dev.* **1964**, *3*, 33 – 38.
[22] F. S. Karn, J. F. Schultz, R. E. Kelly, R. B. Anderson, *Ind. Eng. Chem. Prod. Res. Dev.* **1963**, *2*, 43 – 47.
[23] F. Fischer, H. Tropsch, in *Gesammelte Abhandlungen Zur Kenntnis Der Kohle* (Ed.: F. Fischer), Gebrüder Borntraiger, Berlin, **1932**, pp. 313 – 501.
[24] A. J. McCue, J. A. Anderson, *Catal. Sci. Technol.* **2014**, *4*, 272.
[25] R. J. Madon, H. Seaw, *Catal. Rev.* **1977**, *15*, 69 – 106.
[26] Improvements in the Manufacture and Production of Unsaturated Hydrocarbons of Low Boiling Point, **1929**, GB322284.
[27] J. A. Kritzinger, *Catal. Today* **2002**, *71*, 307 – 318.
[28] H. M. Torres Galvis, A. C. J. Koeken, J. H. Bitter, T. Davidian, M. Ruitenbeek, A. I. Dugulan, K. P. De Jong, *J. Catal.* **2013**, *303*, 22 – 30.
[29] H. M. Torres Galvis, A. C. J. Koeken, J. H. Bitter, T. Davidian, M. Ruitenbeek, A. I. Dugulan, K. P. De Jong, *Catal. Today* **2013**, *215*, 95 – 102.
[30] H. M. Torres Galvis, J. H. Bitter, C. B. Khare, M. Ruitenbeek, A. I. Dugulan, K. P. de Jong, *Science* **2012**, *335*, 835 – 838.
[31] H. M. Torres Galvis, Direct Production of Lower Olefins from Synthesis Gas Using Supported Iron Catalysts, PhD Thesis, **2013**, Utrecht University.
[32] V. R. Calderone, N. R. Shiju, D. C. Ferré, G. Rothenberg, *Green Chem.* **2011**, *13*, 1950.
[33] H. Arai, K. Mitsuishi, T. Seiyama, *Chem. Lett.* **1984**, *13*, 1291 – 1294.
[34] V. A. de la Peña O'Shea, M. C. Álvarez-Galván, J. M. Campos-Martín, J. L. G. Fierro, *Appl. Catal. A* **2007**, *326*, 65 – 73.
[35] Y. Bi, A. K. Dalai, *Can. J. Chem. Eng.* **2008**, *81*, 230 – 242.
[36] S. Lögdberg, D. Tristantini, Ø. Borg, L. Ilver, B. Gevert, S. Järås, E. A. Blekkan, A. Holmen, *Appl. Catal. B* **2009**, *89*, 167 – 182; and references therein.
[37] T. Das, G. Deo, *J. Phys. Chem. C* **2012**, *116*, 20812 – 20819.
[38] A. Griboval-Constant, A. Butel, V. V. Ordomsky, P. A. Chernavskii, A. Y. Khodakov, *Appl. Catal. A* **2014**, *481*, 116 – 126; and references therein.
[39] P. Mondal, G. S. Dang, M. O. Garg, *Fuel Process. Technol.* **2011**, *92*, 1395 – 1670.
[40] P. Raybaud, G. Kresse, J. Hafner, H. Toulhoat, *J. Phys. Condens. Matter* **1997**, *9*, 11085 – 11106.
[41] C. G. Visconti, L. Lietti, P. Forzatti, R. Zennaro, *Appl. Catal. A* **2007**, *330*, 49 – 56.
[42] S. S. Pansare, J. D. Allison, *Appl. Catal. A* **2010**, *387*, 224 – 230.
[43] S. Rane, Ø. Borg, J. Yang, E. Rytter, A. Holmen, *Appl. Catal. A* **2010**, *388*, 160 – 167.
[44] D. E. Sparks, G. Jacobs, M. K. Gnanamani, V. R. R. Pendyala, W. Ma, J. Kang, W. D. Shafer, R. A. Keogh, U. M. Graham, P. Gao, B. H. Davis, *Catal. Today* **2013**, *215*, 67 – 72.
[45] C. H. Bartholomew, R. M. Bowman, *Appl. Catal.* **1985**, *15*, 59 – 67.
[46] D. J. J. Duvenhage, N. J. J. Coville, *Appl. Catal. A* **1997**, *153*, 43 – 67.
[47] H. Pines, W. O. Haag, *J. Am. Chem. Soc.* **1960**, *82*, 2471 – 2483.
[48] W. O. Haag, H. Pines, *J. Am. Chem. Soc.* **1960**, *82*, 2488 – 2494.
[49] J. J. H. B. Sattler, J. Ruiz-Martinez, E. Santillan-Jimenez, B. M. Weckhuysen, *Chem. Rev.* **2014**, *114*, 10613 – 10653.
[50] J. Zhang, X. Liu, R. Blume, A. Zhang, R. Schlögl, D. S. Su, *Science* **2008**, *322*, 73 – 77.
[51] J. Haber, E. Lalik, *Catal. Today* **1997**, *33*, 119 – 137.
[52] L. M. Madeira, M. F. Portela, *Catal. Rev.* **2002**, *44*, 247 – 286.
[53] H. H. Kung, *Adv. Catal.* **1994**, *40*, 1 – 38.
[54] F. Kapteijn, *J. Catal.* **1994**, *150*, 94 – 104.
[55] F. Morales, F. M. F. de Groot, P. Glatzel, E. Kleimenov, H. Bluhm, M. Hävecker, A. Knop-Gericke, B. M. Weckhuysen, *J. Phys. Chem. B* **2004**, *108*, 16201 – 16207.
[56] F. Morales, E. de Smit, F. M. F. de Groot, T. Visser, B. M. Weckhuysen, *J. Catal.* **2007**, *246*, 91 – 99.
[57] C. Ratnasamy, J. P. Wagner, *Catal. Rev.* **2009**, *51*, 325 – 440.
[58] G. Subías, V. Cuartero, J. García, J. Blasco, O. Mathon, S. Pascarelli, *J. Phys. Conf. Ser.* **2009**, *190*, 012089.
[59] Y. Liu, F. Meirer, P. A. Williams, J. Wang, J. C. Andrews, P. Pianetta, *J. Synchrotron Radiat.* **2012**, *19*, 281 – 287.
[60] I. D. Gonzalez-Jimenez, K. Cats, T. Davidian, M. Ruitenbeek, F. Meirer, Y. Liu, J. Nelson, J. C. Andrews, P. Pianetta, F. M. F. de Groot, B. M. Weckhuysen., *Angew. Chem. Int. Ed.* **2012**, *51*, 11986 – 11990; *Angew. Chem.* **2012**, *124*, 12152 – 12156.
[61] a) K. H. Cats, I. D. Gonzalez-Jimenez, Y. Liu, J. Nelson, D. van Campen, F. Meirer, A. M. J. van der Eerden, F. M. F. de Groot, J. C. Andrews, B. M. Weckhuysen, *Chem. Commun.* **2013**, *49*, 4622 – 4624; b) K. H. Cats, J. C. Andrews, O. Stephan, K. March, C. Karunakaran, F. Meirer, F. M. F. de Groot, B. M. Weckhuysen, *Catal. Sci. Technol.* **2016**, *6*, 4438 – 4449.

 © 2018 The Authors. Published by Wiley-VCH Verlag GmbH & Co. KGaA, Weinheim

[62] J. C. Andrews, B. M. Weckhuysen, *ChemPhysChem* **2013**, *14*, 3655 – 3666.
[63] K. H. Cats, B. M. Weckhuysen, *ChemCatChem* **2016**, *8*, 1531 – 1542.
[64] F. Morales, F. M. F. de Groot, O. L. J. Gijzeman, A. Mens, O. Stephan, B. M. Weckhuysen, *J. Catal.* **2005**, *230*, 301 – 308.
[65] F. Morales, D. Grandjean, F. M. F. de Groot, O. Stephan, B. M. Weckhuysen, *Phys. Chem. Chem. Phys.* **2005**, *7*, 568 – 572.
[66] Z. Zhang, W. Dai, X. C. Xu, J. Zhang, B. Shi, J. Xu, W. Tu, J. F. Han, *AIChE J.* **2017**, *63*, 4451 – 4464.
[67] J. Zheng, J. Cai, F. Jiang, Y. B. Xu, X. H. Liu, *Catal. Sci. Technol.* **2017**, *7*, 4736 – 4755.
[68] a) L. S. Zhong, F. Yu, Y. L. An, Y. Zhao, Y. H. Sun, Z. J. Li, T. J. Lin, Y. J. Lin, X. Z. Qi, Y. Y. Dai, L. Gu, J. S. Hu, S. F. Jin, Q. Shen, H. Wang, *Nature* **2016**, *538*, 84 – 87; b) Z. J. Li, T. J. Lin, F. Yu, Y. L. An, Y. Y. Dan, S. G. Li, L. S. Zhuong, H. Wang, P. Gao, Y. H. Sun, M. Y. He, *ACS Catal.* **2017**, *7*, 8023 – 8032.

Manuscript received: September 6, 2017
Version of record online: March 1, 2018

 © 2018 The Authors. Published by Wiley-VCH Verlag GmbH & Co. KGaA, Weinheim